Resonant states of H_3^+ and D_2H^+

Bruno C. Silva, Paolo Barletta, James J. Munro, and Jonathan Tennyson[a)]
Department of Physics and Astronomy, University College London, Gower Street, London WC1E 6BT, United Kingdom

(Received 7 April 2008; accepted 23 May 2008; published online 27 June 2008)

Vibrational resonances for H_3^+ and D_2H^+, as well as H_3^+ at $J=3$, are calculated using a complex absorbing potential (CAP) method with an automated procedure to find stability points in the complex plane. Two different CAP functional forms and different CAP extents are used to analyze the consistency of the results. Calculations are performed using discrete variable representation continuum basis elements calculated to high levels of accuracy by diagonalizing large, dense, Hamiltonian matrices. For D_2H^+, two energy regions are analyzed: the one where D_2+H^+ is the only dissociation product and the one where $HD+D^+$ can also be formed. Branching ratios are obtained in the latter case by using different CAPs. It is shown that H_3^+ and D_2H^+ support some narrow Feshbach-type resonances but that higher angular momentum states must be studied to model the pre-dissociation spectrum recorded by Carrington and co-workers [J. Chem. Phys. **98**, 1073 (1993)]. © *2008 American Institute of Physics*. [DOI: 10.1063/1.2945899]

I. INTRODUCTION

The H_3^+ molecule and its isotopologues are a benchmark system in chemical physics. It is the simplest bound polyatomic molecule, having only two electrons and three nuclei. Hence, it is possible to compute its ground electronic surface up to dissociation[1,2] with high accuracy. Yet, it is hard to obtain a quantitatively and qualitatively satisfactory description of its vibrational-rotational spectrum above 30 000 cm^{-1}, as the nuclear states in this energy region become extremely floppy and the spectrum very dense. H_3^+ also plays a fundamental role in astronomy, being at the root of a series of chemical reactions in the interstellar environment.[3] It has been detected in both diffuse and dense interstellar media, as well as the ionosphere of gas giants.[4]

More than 20 years ago, Carrington and Kennedy performed a remarkable photodissociation experiment on H_3^+ that caught the molecular spectroscopy community by surprise.[5,6] An extremely dense spectrum with about 27 000 individual lines in a frequency range of only 222 cm^{-1} was reported. This was later confirmed in a more refined experiment,[7] which has attracted considerable theoretical interest throughout the years.[8–11]

So far, the only aspect of the recorded spectrum which is fully understood is its behavior with respect to isotopic substitution, whose explanation rests on semiclassical rather than fully quantum mechanical analysis.[12–14] Nevertheless, it is accepted that this spectrum involves transitions between bound and quasibound states near dissociation and with lifetimes ranging from 10^{-9} to 10^{-6} s. Despite attempts to understand the nature of these states,[15] there has been no successful simulation of the spectrum as yet.[16]

A good quantitative description of the spectrum thus requires accurate calculations of both bound and resonant states near dissociation. In previous publications,[11,17,18] results for the bound states of H_3^+ at $J=0$ and $J=3$ and D_2H^+ at $J=0$ were presented. Those calculations employed very large basis sets and were performed at the HPC*x* supercomputer, reaching an overall accuracy of about 1 cm^{-1}.

There is a broad range of methods available to calculate energies and lifetimes of metastable states, categorized as being L^2 or non-L^2. The usage of non-L^2 methods such as the search for poles in the S matrix, or the variational scattering methods[19] in systems such as H_3^+ and D_2H^+, is computationally prohibitive due to the need to calculate the so called bound-free matrix elements. These difficulties are both due to the intrinsic need for large basis sets and to the higher dimensionality of the three-particle problem.[20,21] L^2 methods can reduce the computational requirements but with some cost in accuracy. The most widely used L^2 methods are the stabilization,[22] complex scaling,[23–25] and complex absorbing potential[26] (CAP) methods.

Although all the L^2 methods mentioned can give reliable results, the CAP method was preferred in this work since it can be used with basis elements and energy eigenvalues of these systems, such as the ones obtained in previous calculations performed by this group.[11,17,18] Furthermore, use of the automation procedure implemented here makes it possible to use this method to identify the very large number of resonance states required to model H_3^+ predissociation spectrum.

A step taken toward a better understanding of this problem was the work by Mandelshtam and Taylor[9] who studied resonant states of H_3^+ for $J=0$ using a CAP method.[27] This work attempted to understand the properties of the metastable vibrational states of H_3^+ but used a potential energy surface (PES) designed to accurately produce only the lowest bound states and had an incorrect dissociation limit and missed the R^{-4} term in the asymptotic region.[28]

In this paper, we report accurate calculations of energies and lifetimes of these resonant states, in an energy window just above the dissociation limit. The results presented here

[a)]Electronic mail: j.tennyson@ucl.ac.uk.

were obtained by applying the CAP method to the basis elements obtained from the most accurate dense Hamiltonian matrix diagonalizations of nuclear motion Hamiltonians for these systems to date[11,17,18] using a PES which is accurate up to the dissociation threshold.[2] Results are presented for H_3^+ at $J=0$ and $J=3$ and D_2H^+ at $J=0$ through a new automatic resonance detection procedure which integrates a consistency check and subsequent error estimation.

This paper is structured as follows: Section II outlines the theoretical background and computational details of the vibrational-rotational calculations and CAP method; Section III describes the preliminary test calculations that determine the CAP parameters used in the final calculations. In Sec. IV, the final results are presented and discussed. The conclusions and future work are presented in Sec. V.

II. CAP METHOD

The CAP method involves augmenting the dissociating system's PES with a complex functional form that absorbs the continuum part of the wavefunction. Ideally, this non-Hermitian Hamiltonian will produce L^2 wavefunctions above the dissociation threshold that represent the resonant states in question. Riss and Meyer[29] have studied this method in some depth, providing a basic understanding of the way the CAP affects the spectra of several families of one-dimensional Hamiltonians.

Formally, an imaginary negative potential that acts on the dissociation coordinate R is added to the system's Hamiltonian $\hat{H}$:

$$\hat{H}' = \hat{H} - i\lambda W(R), \tag{1}$$

where λ is a parameter used to control the CAP's intensity. The resulting non-Hermitian Hamiltonian $\hat{H}'$ defines the energy of the nth resonance E_n, its width Γ_n, and the corresponding L^2 wavefunction Ψ_n through the relationship

$$\hat{H}'(\lambda)\Psi_n(\lambda) = \left(E_n(\lambda) - i\frac{\Gamma_n(\lambda)}{2}\right)\Psi_n(\lambda). \tag{2}$$

To solve Eq. (2), $\hat{H}'$ can be projected on a suitable basis and diagonalized. In the infinite basis set limit, the eigenvalues corresponding to the resonant states will be found in the limit where $\lambda \to 0$. Fortunately, the use of a finite basis set is both necessary and beneficial: The error introduced by the CAP and the finite basis set have opposite phases. This implies that these errors will cancel each other out at some optimal value, λ_{op}, thus yielding the complex "observable" associated with the resonant state.

The search for λ_{op} is done by studying the behavior of the complex eigenvalues of Eq. (2) with values of λ ranging from zero to a large arbitrary value. This results in N trajectories in the complex plane, each associated with an eigenvalue $E_n - i\Gamma_n/2$. Through graphical analysis of these trajectories, it is possible to identify the point in the complex plane that corresponds to the optimal value λ_{op}, and hence estimate the value for the position E_n and width Γ_n of the resonant state. This graphical method consists of locating cusps, loops, and stability points in the eigenvalue trajectory, which are known to occur in positions around the true eigenvalue for the resonances on the complex plane.[30]

The approach taken in this work is to first diagonalize $\hat{H}$ of the system under study and store the basis elements ϕ_i and eigenvalues ε_i lying near the dissociation limit. As one can expand the functions Ψ_n of Eq. (2) onto the basis set obtained from the bound state calculation,

$$|\Psi_n(\lambda)\rangle = \sum_i c_n^i(\lambda)|\phi_i\rangle. \tag{3}$$

The coefficients $c_n^i(\lambda)$, the resonance energies $E_n(\lambda)$, and the resonance widths $\Gamma_n(\lambda)/2$ can then be obtained by diagonalizing the Hamiltonian:

$$H'_{ji} = \langle\phi_j|\hat{H}'|\phi_i\rangle = \varepsilon_i\delta_{ji} - i\lambda\langle\phi_j|W(R)|\phi_i\rangle, \tag{4}$$

where ε_i is the ith eigenvalue and ϕ_i is the ith eigenvector obtained from the diagonalization of $\hat{H}$.

Calculations of resonant energies and widths relying solely on the use of minima and maxima in the eigenvalue trajectories were performed by Skokov *et al.*[31] and later on by Mussa and Tennyson[21] to identify resonant states of HOCl, which showed good agreement with experiment.[32]

A. Complex absorbing potentials

The functional form employed in the definition of the CAP is rather arbitrary and depends on a few parameters. Reasonable physical assumptions define a range of choices for those parameters, though resonant energies and positions should not be affected by the specific choice and should show stability with respect to small variations of the parameters. One of these assumptions is that CAP's starting point r_1 should be relatively far inside the dissociation region in order to absorb only the continuum part of the wavefunction. Nevertheless, the choice of parameters is mostly arbitrary, leading to a degree of uncertainty in the results which so far has not been properly quantified. As will be shown later, different r_1 values may lead to different results for both the resonance energy and width, resulting in an absence of consistency between stability points. For this reason, a consistency check was implemented in the calculation. This check involves calculating the resonances for a set of CAPs, differing only in their r_1 positions, probing the consequences of absorbing different regions of the continuum wavefunctions and verifying the validity of any result obtained.

There are a number of complex absorbing potentials available,[33–36] as well as techniques to produce potentials with optimal properties.[27,37] For this reason, we have chosen to study two functional forms of CAP, one for its simplicity and the other for its optimal properties.

The simplest and most commonly employed CAP is the nth order monomial potential given by

$$W_n(R) = \left(\frac{R - r_1}{r_2 - r_1}\right)^n, \quad r_1 \leqslant R < r_2. \tag{5}$$

More formally motivated is the potential due to Manolopoulos.[35] This potential was more recently refined by Gonzalez-Lezana *et al.*[36] (GLM) to

$$W_{\mathrm{GLM}}(R) = \frac{\hbar^2}{2\mu}\left(\frac{2\pi}{r_2 - r_1}\right)^2 y(x), \quad r_1 \leqslant R < r_2, \tag{6}$$

with $y(x)$ approximately given by

$$y(x) = \frac{4}{(c-x)^2} + \frac{4}{(c+x)^2} - \frac{8}{c^2}, \tag{7}$$

where

$$c = \sqrt{2}K(1/\sqrt{2}), \tag{8}$$

and

$$x = c\frac{R - r_1}{r_2 - r_1}, \tag{9}$$

where $K(1/\sqrt{2})$ is a standard elliptic integral. In both these CAPs, r_2 is placed at the end and r_1 at the start of the CAP in the dissociation coordinate R.

The two most interesting features of the GLM CAP are its minimum reflection properties and the common term in Eq. (6) that couples the CAP amplitude to its length, $\Delta r = r_2 - r_1$, as a single parameter for locating the stability points λ_{op}. Unfortunately, due to the method employed in this work, the parameter coupling creates an important difficulty using this CAP: To scan all the necessary energies (amplitudes), one would have to build a new CAP matrix for each amplitude. This would significantly increase computational cost due to the number of energy points required for a detailed search of such a dense spectrum. For this reason, we chose to remove the common term in Eq. (6), replacing it instead with the usual amplitude parameter λ while keeping the optimal form of Eq. (7).

In this work, we have employed both the GLM CAP and the monomial CAP with n set to 2, henceforth referred as the M2 CAP, to test their effect on both the properties of the resonant states and consistency of the results.

The idea that one must test the consistency of the results obtained from the CAP method stems from the assumption that changing the complex absorbing potential should not have a significant effect in the positions and half-widths and from the fact that there is no fundamental physical reason for choosing a particular CAP, apart from setting r_1 at some point "well" inside the open dissociation channel and r_2 at the end of the wavefunction grid.

B. Automatic resonance detection

As discussed in Sec. II, successive diagonalizations with varying values of λ lead to different trajectories in the complex plane. These trajectories must then be inspected one by one. The main difficulty with this approach lies in the fact that to find resonant states one has to inspect thousands of plots and manually identify all the values of λ_{op} for a number of CAP parameters and functions. To alleviate these difficulties, we developed an automated detection procedure that uses the graphical method criteria described above to detect the existence of stability points.

The procedure consists of analyzing the individual trajectories, obtained for a particular $W(R)$ function along increasing values of λ. These are scanned in a search for the nearby occurrence of three conditions. The first condition arises from the existence of a local maximum or a local minimum in the complex energy, as generally occurs in the presence of a loop or a cusp. Second, the same trajectory is tested for the existence of stability regions where the density of points along the trajectory has a maximum. This can be stated as

$$\frac{dN_E}{dl} = 0, \quad \frac{d^2N_E}{dl^2} < 0, \tag{10}$$

where N_E is the number of complex energy points per unit of trajectory length and l is the position along the trajectory. Finally, the existence of maxima in the trajectory's curvature is tested, with the curvature κ given by

$$\kappa(\lambda) = \frac{|E'(\lambda)\Gamma''(\lambda) - \Gamma'(\lambda)E''(\lambda)|}{(\Gamma'(\lambda)^2 + E'(\lambda)^2)^{3/2}}. \tag{11}$$

The next step is to identify which λ values satisfy all three conditions within a certain tolerance window. If all three conditions occur within that window, a successful detection of a stability point is flagged. Each successful detection is then recorded. With this information, it is now possible to assess the uncertainty associated with the choice of r_1 and identify which results are truly consistent.

Spurious detections may arise in two situations. First, if the CAP range Δr is insufficiently long, then the CAP functional form will be inadequately sampled, thus leading to the introduction of an error. Second, if Δr is too long, parts of the wavefunction that are close to the potential well will be overabsorbed by the CAP which will significantly affect the position and width of the detection.

To remove these spurious identifications, an iterative procedure removes all stability point detections that produce a large deviation from the average of the norm of the complex energy. The procedure goes as follows: The average of the stability points found over all tested r_1 values is calculated; the deviation from the average for each stability point is computed; the average is recalculated excluding the stability point with largest deviation and that lies outside the tolerance window; the process is repeated until no stability points can be excluded; and finally, the largest deviation from the average complex energy that lies inside the tolerance window is given as the uncertainty, and a percentage of detection is then calculated from the fraction of points selected over all the tested r_1 values.

III. CALCULATIONS

A. PDVR3D energy level calculations

Full diagonalizations of the Hamiltonians for H_3^+ (Refs. 11 and 17) with angular momentum $J=0$ and $J=3$ and D_2H^+ (Ref. 18) with $J=0$ were performed using a parallel implementation of the DVR3D (Ref. 38) suite for the calculation of the spectra of triatomic molecules, named PDVR3D. The nuclear Hamiltonian constructed in this program describes the system in Radau coordinates with the laboratory referential z axis perpendicular to the molecular plane.[39,40] An improved version[41] of this code was implemented on HPCx.[42] These calculations use a PES (Ref. 2) that correctly describes

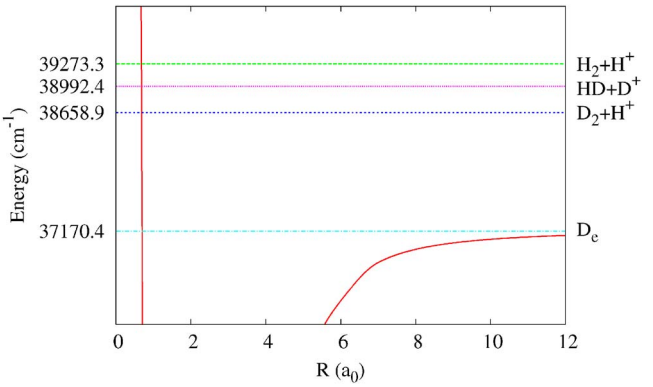

FIG. 1. (Color online) Dissociation thresholds of H_3^+ and D_2H^+ calculated on the potential energy surface used in this work. The dissociation limits lie above D_e by the zero point energies of the respective diatomic fragments. These energies were calculated using LEVEL 7.5 (Ref. 50). The energy limits are plotted against a cut of the potential energy surface along the dissociation coordinate and with diatomic internuclear distance set to equilibrium of H_2. The energy zero is set to the bottom of the potential.

the dissociation regions of the H_3^+ system. A correction to this PES was later on introduced to remove a small unphysical artifact.[11] This surface is henceforth referred to as PPKT2. Although other global PESs for H_3^+ have been reported,[43,44] these are aimed at both ground and excited states, and it is not clear that they are as accurate for the ground state. Unfortunately, lack of computer resources prevented comparative tests using these surfaces.

Originally, the H_3^+ calculations were performed with a grid defined by 96 angular points and 120 radial points in Radau coordinates with C_{2v}, and not the natural D_{3h} spacial symmetry. This causes E states in the D_{3h} symmetry group to appear repeated as A_1 and B_1 states from the C_{2v} group. Note that, due to the Pauli principle, only the states in the B_1 symmetry block are physically allowed for H_3^+. The radial basis functions were constructed from spherical oscillators[38] with basis parameters $\alpha=0$, $\omega=0.004$ E_h. In the final H_3^+ calculations, the three-dimensional (3D) Hamiltonian size was 79 091, with states converged within 1 cm^{-1}.[17] The same basis set parameters used for the calculation of H_3^+ were used as the starting point for the D_2H^+ calculations, leading to a final 3D Hamiltonian size of 122 000, giving bound states converged within about 0.1 cm^{-1}. This level of convergence is significant since the density of states in D_2H^+ is approximately twice that of H_3^+.[18]

To improve upon those results and to provide a measure of convergence for the resonance calculations, two new calculations for both D_2H^+ and H_3^+ were performed. The largest calculation of D_2H^+ at $J=0$ was made increasing the radial grid size to 130 points and setting the final Hamiltonian to a size of 124 818. These calculations achieved an energy convergence to 0.05 cm^{-1}. The largest vibrational H_3^+ calculations were performed with the radial grid size extended to 140 points and a final 3D Hamiltonian of 94 224, giving energy states converged to about 0.1 cm^{-1}. These convergence values determine lower limits for convergence of the D_2H^+ and H_3^+ resonant states presented in Tables IV and VI, respectively.

An important side effect of changing the number of radial grid points is a change in the overall grid box size. In H_3^+, changing the number of grid points from 120 to 140 moved the outermost grid point, i.e., the furthest point in the Jacobi dissociation coordinate, R_3, for any angle, as given in Fig. 2, from 19.91 to 21.56 a_0. Similarly in D_2H^+, changing the number of radial grid points from 120 to 130 moved the furthest R_3 point from 20.70 to 21.58 a_0. Thus, the convergence tests incorporate the effect of changing the grid box size. We note that the grid points are not evenly distributed but are concentrated at short and intermediate distances and become sparser at large distances.

Similar calculations were performed for H_3^+ at $J=3$ using the same basis set parameters and size as the first $J=0$ calculation, but at a very high computational cost: Approximately 45 000 CPU hours.[41] This computational cost prevented the calculation of other rotational states and the full convergence analysis of H_3^+ at $J=3$. However, based upon the results for $J=0$, we believe that these states are converged to a similar level of accuracy.

B. CAP method parameters

To assess how the CAP forms and parameters influence the results, tests were performed using D_2H^+ wavefunctions. This choice comes from the fact that this system allows the study of both single and multichannel dissociation through two contiguous energy regions. Figure 1 illustrates the different dissociation thresholds for D_2H^+ and H_3^+ plotted against the PPKT2 PES. Between 38 659 and 38 992 cm^{-1}, only dissociation of a proton can occur, with the dissociation coordinate being R_3. Above 38 992 cm^{-1}, D_2H^+ can dissociate into both D^++HD through R_1 and R_2 and H^++D_2 through R_3. In these tests, we have also restricted ourselves to the calculation of resonances with A_1 symmetry since these are the hardest to converge.

In the case where the system has symmetry, the CAP is applied to all the symmetric channels by embedding the coordinate system appropriately, as illustrated in Fig. 2. In the case of H_3^+, this is written as

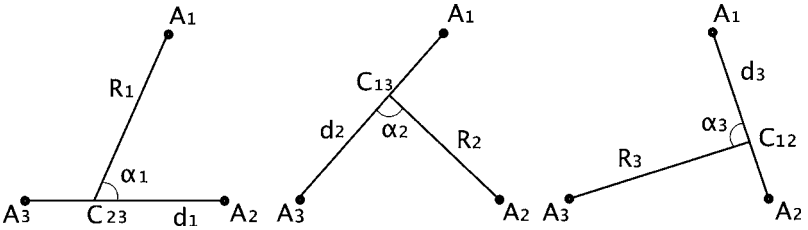

FIG. 2. Diagram representing the three possible choices of the Jacobi coordinate system (d_i, R_i, α_i), where d_i is the diatom internuclear distance, R_i is the dissociation coordinate with origin at the diatomic center of mass, C_i, and α_i is the dissociation angle.

TABLE I. Sample of resonance positions E and half-widths $\Gamma/2$ in cm^{-1} obtained directly from the automatic stability point detection method for the GLM CAP for a set of 5 Δr values, ranging from 4 to 8 a_0 with r_2 set at 21.58 a_0. Powers of 10 are given in parentheses.

Δr=4.0 a_0		5.0 a_0		6.0 a_0		7.0 a_0		8.0 a_0	
E	$\Gamma/2$	E	$\Gamma/2$	E	$\Gamma/2$	E	$\Gamma/2$	E	$\Gamma/2$
						38 724.69	3.15(0)	38 724.83	3.16(0)
		38 729.28	2.95(−1)	38 728.67	5.53(−1)	38 728.70	5.54(−1)	38 728.70	5.73(−1)
						38 735.20	1.47(1)	38 735.93	1.63(1)
38 739.99	9.33(−1)	38 739.83	1.18(0)			38 739.73	1.20(0)	38 739.71	1.20(0)
38 743.70	1.74(−1)	38 743.68	2.12(−1)			38 743.67	2.16(−1)	38 743.67	2.15(−1)
		38 753.23	7.31(−6)	38 753.23	7.71(−6)	38 753.23	7.77(−6)	38 753.23	7.94(−6)
		38 760.54	1.80(−1)	38 760.55	1.76(−1)	38 760.55	1.76(−1)	38 760.55	1.76(−1),
38 762.27	2.57(−1)	38 762.27	2.22(−1)	38 762.28	2.19(−1)	38 762.28	2.19(−1)	38 762.28	2.19(−1)
38 773.53	2.49(−1)	38 773.68	9.28(−2)	38 773.50	2.62(−1)	38 773.50	2.61(−1)	38 773.50	2.59(−1)
38 785.13	3.22(−1)	38 785.14	3.69(−1)	38 785.14	3.72(−1)	38 785.14	3.74(−1)	38 785.13	3.74(−1)
		38 791.87	2.77(−1)	38 791.88	2.79(−1)	38 791.88	2.80(−1)	38 791.88	2.81(−1)
38 797.40	1.30(−1)	38 797.41	1.22(−1)	38 797.41	1.22(−1)	38 797.41	1.22(−1)	38 797.41	1.22(−1)
38 805.01	3.44(−1)	38 804.61	1.16(0)	38 804.61	1.16(0)	38 804.61	1.15(0)	38 804.61	1.16(0)
		38 811.89	2.82(−2)	38 811.89	2.84(−2)	38 811.89	2.84(−2)	38 811.89	2.90(−2)
38 815.92	6.68(−1)	38 815.89	6.88(−1)	38 815.88	6.95(−1)	38 815.88	6.94(−1)	38 815.88	6.99(−1)
38 820.23	7.42(−1)	38 820.20	7.64(−1)	38 820.20	7.73(−1)	38 820.19	7.74(−1)	38 820.19	7.87(−1)
		38 830.02	4.89(−2)	38 830.02	4.87(−2)	38 830.02	4.88(−2)	38 830.02	4.86(−2)
		38 837.83	2.20(0)						
38 838.30	1.80(0)	38 837.83	2.20(0)	38 837.88	2.18(0)	38 837.92	2.22(0)	38 838.22	2.10(0)
38 841.61	3.45(−1)	38 841.76	4.46(−1)	38 842.38	6.60(−1)	38 843.47	1.01(0)	38 845.48	8.97(−1)

$$\hat{H}' = \hat{H} - i\lambda \sum_{i=1}^{3} W(R_i), \tag{12}$$

where i runs over the number of symmetric channels, which is 3 for H_3^+. In the D_2H^+ case,

$$\hat{H}' = \hat{H} - i\lambda (W(R_1) + W(R_2) + V(R_3)), \tag{13}$$

where the potentials W and V have the same functional form but with different choices of the parameter r_2.

This approach leads to a question in the case where the representation of the wavefunction is made in a symmetry lower then that of the potential: For H_3^+, which has D_{3h} symmetry, the dissociation of all three hydrogen atoms would be equally represented by the three possible Jacobi coordinate transformations. With a C_{2v} representation in Radau coordinates, the three transformations to Jacobi coordinates lead to shorter and sparser grids on two of the coordinate systems. For example, R_3 as described in Fig. 2, and with the wavefunction parameters set for the calculation of highest convergence, we obtain a maximum of 21.56 a_0 where as for R_1 and R_2 we obtain 18.64 a_0. Because the difference in extent is only about 10%, we chose to set the total CAP to r_2 at 21.56 a_0 and use the same extent Δr for all channels.

When doing the convergence tests, the most significant change in the number of grid points was done for H_3^+. Changing from 120 to 140 radial points in Radau coordinates changes the position of r_2 from 19.91 to 21.56 a_0 in the Jacobi dissociation coordinate R_3, whereas r_2 changes from 17.24 to 18.67 a_0 in R_1 and R_2. The differences are fairly small in both dissociation channels. Since the radial grid change in the vibrational D_2H^+ calculations is even smaller, the same set of Δr values are used in the consistency analysis of the wavefunction basis convergence tests.

1. λ grid

There is a clearly defined window for the lifetime of resonant states that may participate in the predissociation spectrum that arises from the physical dimensions of the Carrington-Kennedy experimental apparatus. The lower and upper limits for the lifetimes are given by time the ions in these resonant states take to travel from their origin to the start and the end of the drift tube, respectively, since the drift tube is where the dissociation must occur to be detected. The time that an ion takes to travel from the ion source to the laser is of the order of 10^{-6} s.[7] This means that the initial state must have a maximum width of about 10^{-6} cm^{-1}. Detection of the dissociation product is sensitive to final states with lifetimes between 10^{-9} and 10^{-7} s, respectively. This sets the final state resonance widths approximately between 10^{-5} and 10^{-3} cm^{-1}. Due to this broad width window, the λ grid must obey three constraints: It must cover all the relevant CAP intensities that map the positions of the stability points with Γ between 10^{-5} and 10^{-3} cm^{-1}; it must be sufficiently dense to describe the stability points in detail; and the differences between the grid points must be small so that the eigenvectors can be matched at each step. This last point is particularly important since the eigenvalues often change their ordering as λ increases, reflecting the existence of crossings between trajectories. The trajectory tracking is achieved by doing a normalized scalar product between all the complex eigenvectors in every two successive λ steps. It is desirable for all these constraints to be met with minimum computational cost.

To cover the resonance space appropriately at both low and high energy ranges and to allow for a finer control of the grid progression, we have chosen to use an exponential function balanced by a fraction for λ, as given by

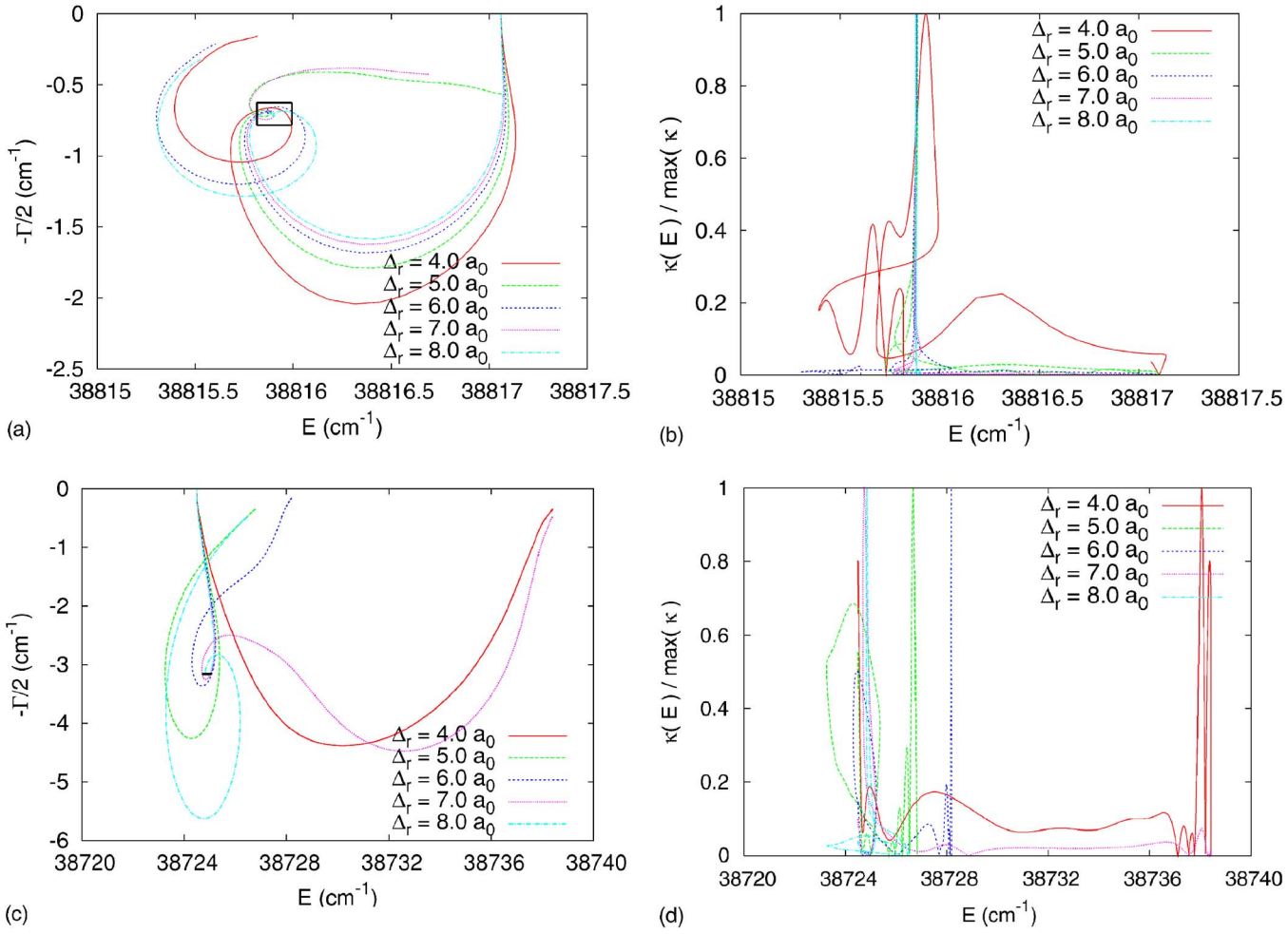

FIG. 3. (Color online) Sample of trajectories in the complex energy plane and their curvatures, generated using the GML CAP for A_1 basis elements, for Δ_r from 4 to 8 a_0 in steps of 1 a_0, and with λ from of 0 to 2×10^5 cm^{-1}. The plots indicate (a) a resonance at 38 815.90 cm^{-1} with $\Gamma/2=0.70$ cm^{-1} and (b) an inconsistent resonance at 38 724.87 cm^{-1} with $\Gamma/2=3.16$ cm^{-1}. The black squares are the detection results, centered at the averaged real and imaginary parts of the eigenvalue, with sides indicating the maximum deviation in the detected stability points for the total of five CAPs used. (c) and (d) are the respective normalized curvatures with respect to the resonant energy. The detection percentage in case (a) was 77.8% and in case (b) was 44.4%.

$$\lambda_n = h\frac{\chi^n - 1}{\chi - 1}, \quad n = 0, \ldots, N, \tag{14}$$

where h has units of energy and is used to establish the order of magnitude, χ is the progression parameter, and there are $N+1$ grid points.

For both D_2H^+ and H_3^+, we have found that the parameters $\chi=1.01$ and $h=4.39\times10^{-2}$ cm^{-1}, giving a maximum amplitude of 2.41×10^5 cm^{-1} at 1100 points, are sufficient to cover the complex plane for all the eigenvalues tested.

2. Automatic detection

The detection algorithm was calibrated by setting four parameters. The first two are the tolerance window for the occurrence of the different detection stability point conditions discussed in Sec. II B. Since an accuracy of about 0.1 cm^{-1} is desired, the maximum distance allowed between the existence of points that satisfy those criteria in the real axis was set to this value. The imaginary energy range covered by the trajectories varies by orders of magnitude from eigenvalue to eigenvalue. For this reason, tolerance for this component is given as a percentage of the total imaginary energy. We have found that a tolerance of 3% produces consistent results.

The second two parameters control the consistency tolerance between the different stability points detected across all the tested r_1 values for a particular resonant eigenvalue, as discussed in the end of Sec. II B. We found that defining these parameters as 0.1 cm^{-1} for the real part of the energy and 15% was adequate to eliminate spurious detections.

3. CAP consistency

Two sets of consistency tests were performed: The first to verify that the results are actually consistent for different r_1 positions, i.e., different CAP lengths Δr, with a single functional form, and the second to test the GLM against the M2 CAPs. All calculations in this section were performed using all the available continuum basis elements from the most converged vibrational D_2H^+ calculation of[18] in the interval 38 724–38 842 cm^{-1} as well as a few bound-region basis elements for testing purposes. r_1 consistency test is shown in Table I. These results indicate that for a particular number of states, changing the range covered by the complex

TABLE II. Comparison of states with half-widths less than 0.15 cm^{-1}, obtained with the GLM and M2 CAPs for a common set of parameters for D_2H^+ $J=0$ A_1 symmetry calculations. "%" represents the percentage of successful detections over all the nine values of Δr from 2 to 10 a_0. E and $\Gamma/2$ in cm^{-1} are averages after removal of spurious detections. ΔE and $\Delta\Gamma/2$ are error in cm^{-1} of energy and half-widths, respectively. Powers of 10 are given in parentheses.

GLM					M2				
%	E	$\Gamma/2$	ΔE	$\Delta\Gamma/2$	%	E	$\Gamma/2$	ΔE	$\Delta\Gamma/2$
66.7	38 685.19	5.34(−6)	0.00	3.93(−6)	77.8	38 685.19	5.16(−6)	0.00	5.57(−6)
88.9	38 753.24	6.88(−6)	0.00	3.01(−6)	55.6	38 753.24	6.99(−6)	0.00	3.21(−6)
77.8	38 797.41	1.24(−1)	0.01	8.24(−3)	66.7	38 797.41	1.21(−1)	0.01	4.65(−3)
55.6	38 811.89	2.71(−2)	0.00	5.83(−3)	77.8	38 811.89	3.04(−2)	0.00	6.89(−3)
66.7	38 830.03	4.76(−2)	0.01	3.81(−3)	77.8	38 830.02	4.85(−2)	0.00	2.86(−3)
66.7	38 891.22	8.17(−2)	0.02	1.03(−2)	44.4	38 891.23	8.53(−2)	0.01	1.75(−2)
77.8	38 918.41	1.22(−1)	0.05	1.69(−2)	88.9	38 918.41	1.28(−1)	0.05	1.86(−2)
88.9	39 058.55	1.47(−1)	0.01	4.73(−3)	77.8	39 058.55	1.45(−1)	0.00	3.61(−3)
77.8	39 074.43	1.77(−2)	0.00	1.73(−4)	77.8	39 074.43	1.80(−2)	0.00	2.94(−3)
88.9	39 119.14	4.08(−2)	0.00	2.06(−3)	88.9	39 119.14	4.03(−2)	0.00	5.15(−3)
88.9	−39 129.46	1.96(−2)	0.00	4.67(−4)	77.8	39 129.46	1.92(−2)	0.00	2.44(−3)
88.9	39 186.83	8.43(−2)	0.00	3.92(−3)	77.8	39 186.83	8.35(−2)	0.01	1.46(−3)
22.2	39 291.15	5.87(−2)	0.06	1.86(−3)					
55.6	39 460.37	1.20(−1)	0.00	2.19(−4)	88.9	39 460.31	7.14(−2)	0.09	1.19(−2)
22.2	39 927.57	1.39(−1)	0.00	1.03(−2)					

absorbing potential has an effect on the detection of resonances. However, more importantly, there is a high level of consistency across most detections.

The differences between consistent and inconsistent states can be better understood through Fig. 3, which illustrates the detection of trajectories in the complex energy plane using five GLM CAP with Δr values from 2 to 10 a_0. By simple visual inspection, it can be seen in case (a) that the trajectories are consistent in the position of the stability points and peaks in curvature, whereas in case (b) the position of the stability points and curvature peaks changes significantly with Δr, suggesting that this result may not be reliable. In fact, the rate of detection given by the automated procedure is 77.8% in case (a), whereas in case (b) it was 44.4%, which is in accordance with these observations.

A common feature in these two cases is that the trajectory associated with $\Delta r=4$ a_0 appears to have a much lower maximum curvature then other trajectories. This is also observed for all trajectories with $\Delta r \leqslant 4$ a_0 and for other eigenvalues as well. In practice, only 0.0008% of the grid points are sampled by CAPs with $\Delta r \leqslant 4$ a_0 which are clearly not enough for the eigenvalue trajectory calculation to be reliable. An interesting example is that of the very narrow resonance positioned at 38 753.23 cm^{-1}, in Table I, which has a very consistent detection throughout all CAP's with $\Delta r > 4$ a_0, but apparently no detection for $\Delta r \leqslant 4$ a_0. As will be shown later in Sec. IV A, this is caused by the fact that the basis elements that contribute to this resonant state have amplitudes close to zero at large distance spatial grid points which introduces an additional numerical error for small Δr.

The consistency of results between the GLM and M2 CAPs was also tested. The results are shown in Table II and indicate that, with the exception of the state with energy 39 460 cm^{-1} where the detection procedure converged to what appear to be local minima that were differently emphasized by each CAP, there is a remarkable consistency in both positions and widths of the calculated resonant states with energies up to 39 187 cm^{-1}. The GLM CAP has a slightly higher detection rate in most cases, giving results which are more consistent as a function of r_1. Also, its optimum transmission properties allow the use of a smaller λ range of values to build the trajectories that lead to detections. For these reasons, all final results were calculated using the GLM CAP.

C. D_2H^+ partial widths

In the case of multidissociation channel systems such as D_2H^+, the total reaction rate is the sum of the reaction rates through each open reaction channel, i.e., the total probability of dissociation is the sum of the probabilities of dissociation through all possible channels at a given energy. This would imply that the linewidths associated with a particular dissociation channel at energies above the threshold should add up to the total linewidth of the system at that same energy. Verification of this property in these resonant calculations is an important indicator in the reliability of the method. To test this, a calculation was performed using a GLM CAP applied separately to the $H^+ + D_2$ and $D^+ + HD$ dissociation channels. Δr was set to 6 a_0 and the basis functions have the same properties as described in the tests above. The results after matching closest resonance energies detected for each dissociation channel are presented in Table III.

From these results, it can be seen that, in all except two cases, the sum of the partial widths equals the total width obtained using a single CAP for all dissociation channels to within about 30%. The resonance energies obtained vary by about 0.5 cm^{-1}. These discrepancies are probably because the optimal λ value for each channel is coupled, as described by Eq. (13), leading to a mismatch between the stability points in the separate channels. Decoupling the λ parameter could possibly solve this problem. However, the implementation of this idea is computationally costly. When the CAP is applied solely to the $D^+ + HD$ dissociation channel, some

TABLE III. Resonant energies and half-widths in cm^{-1} for the $H^+ + D_2$, $D^+ + HD$ and total dissociation above the $D^+ + HD$ threshold. This calculation was performed using the GLM CAP with $\Delta r = 6\ a_0$ for all dissociation channels and r_2 set to the grid limit of both $H^+ + D_2$ and $D^+ + HD$ dissociation channels at 21. 58 and 16. 09 a_0, respectively. $\Delta\Gamma/2$ is the difference between the sum of the partial widths and calculated total width. Powers of 10 are given in parentheses.

$H^+ + D_2$		$D^+ + HD$		All		
E	$\Gamma/2$	E	$\Gamma/2$	E	$\Gamma/2$	$\lvert\Delta\Gamma/2\rvert$
39 019.59	1.15(0)	39 019.89	3.02(0)	39 018.01	4.00(0)	1.74(−1)
39 022.70	1.64(0)	39 022.89	2.68(−2)	39 023.02	1.32(0)	3.44(−1)
39 036.86	9.03(−1)	39 035.42	1.46(0)	39 036.53	3.34(0)	9.75(−1)
39 074.43	1.78(−2)	39 074.94	3.68(1)	39 075.71	3.70(1)	1.69(−1)
39 089.82	3.46(−1)	39 089.08	2.17(−1)	39 089.08	3.69(−1)	1.93(−1)
39 097.50	2.30(0)	39 095.36	1.01(0)	39 098.00	3.62(0)	3.09(−1)
39 125.95	8.93(−1)	39 125.27	3.42(−1)	39 125.44	1.50(0)	2.63(−1)
39 136.19	6.69(−1)	39 136.89	1.58(−1)	39 136.08	9.11(−1)	8.31(−2)
39 145.27	1.84(0)	39 144.69	9.58(−3)	39 144.72	1.24(0)	6.08(−1)
39 170.62	4.23(−1)	39 171.18	2.06(0)	39 171.73	2.77(0)	2.91(−1)
39 175.31	3.50(0)	39 174.21	1.53(0)	39 175.16	5.64(0)	6.08(−1)

widths differ by orders of magnitude on changing the wavefunction basis from 120 to 130 radial grid points. This maybe because Radau coordinates do not permit a complete sampling of the $D^+ + HD$ dissociation regions of the potential, leading to difficulties in terms of convergence when adapting the CAP to all dissociation channels simultaneously. Nevertheless, acceptable results can be obtained by restricting Δr in the total CAP to lengths from 4 to 8 a_0. This makes Δr large enough to cover sufficient grid points in the $D^+ + HD$ channel and short enough not to go too close to the potential well.

D. The role of bound vibrational states

Our method involves neglecting nearly all the bound vibrational states when diagonalizing the CAP Hamiltonian. This assumption needs to be tested, particularly because of the presence of asymptotic vibrational states (AVS),[17] which extend far into the dissociation region where the CAP is placed. In fact, we have found that the effect of the AVS is negligible: Only for one $H^+ + D_2$ resonant state the effect is significant, showing a difference of 0.16 cm^{-1} in energy and 1.75×10^{-2} cm^{-1} in width between the calculations with and without AVSs, while the remaining states differ by less then 0.01 cm^{-1} in energy and 10% in width. This leads to the conclusion that, from the technical point of view of including these states in the CAP calculation, the AVS and all other bound states show negligible coupling to the resonant states and therefore are excluded from the final calculations. Nevertheless, it must be noted that a link of orthogonality between resonant states and AVS exists. In fact, the basis elements above dissociation depend strongly upon the convergence of the bound states for their position, and due to their extension, the AVS are particularly difficult to converge.

IV. RESULTS AND DISCUSSION

Apart from the technical issues inherent to the CAP method as described in Sec. III, there are two more aspects determining how accurate the results are for a given PES. The first aspect is the number of basis elements used to build the CAP matrix, and the second is the size of the basis set used to build these basis elements. The results presented here show how these two parameters influence the final resonance energies and widths. In terms of the CAP basis convergence, the smallest calculations only use basis elements that lie within the relevant resonance energy window, as discussed in Sec. II, and the intermediate step will be half way in between that number and the maximum available.

A. D_2H^+ vibrational resonances

The final results for $J=0$ D_2H^+ candidate resonances are presented in Table IV for both the $H^+ + D_2$ and $D^+ + HD$ dissociation channels as well as the convergence relative to the CAP basis and the wavefunction basis. The results were obtained using 519 A_1 states and 485 B_1 states lying between 38 658 and 41 029 cm^{-1}. Due to the grid constraints imposed by the $D^+ + HD$ dissociation channel, as described in the end of Sec. III B, five CAPs with the GLM functional form were used with Δr ranging from 4 to 8 a_0 in steps of 1 a_0 with r_2 placed at the end of the grid of each respective channel.

A total of 384 candidate resonances with width less than 100 cm^{-1} were detected in the range 38 658–39 658 cm^{-1}, of which 131 have a consistency in Δr above 60%. Detections in the same energy range with half-widths narrower than 0.1 cm^{-1} are presented in Table IV. Table IV shows that there are D_2H^+ resonant vibrational states narrow enough to play a role in the predissociation spectrum for this system, which is somewhat surprising since these Feshbach-type resonances, which arise through energy trapping in the asymmetric stretch and bending degrees of freedom,[45] are usually assumed to be broader.[10,46,47]

As expected,[21] the resonance widths systematically become narrower as either the CAP or wavefunction basis is increased. Two states, in particular, result in very narrow widths, namely, states 3 and 11, both with A_1 symmetry. Very narrow widths in these states suggest that λ_{op} is very small,

TABLE IV. Results and convergence for the D_2H^+ candidate resonant states using a CAP adapted to both the $H^+ + D_2$ and $D^+ + HD$ dissociation channels. The states that are within the lifetimes of the observed predissociation spectrum are in boldface. The columns are position of the resonance E, uncertainty in the position due to consistency ΔE, resonance half-width $\Gamma/2$, uncertainty in half-width due to consistency $\Delta\Gamma/2$, and detection percentage %. For the convergence of results, δE and $\delta\Gamma/2$ are the difference between the largest calculation and the respective lower convergence calculation for the energy and half-widths, respectively: the subscript "a" indicates a CAP eigenvector cutoff at 40 765 cm^{-1} and the subscript "b" indicates a cutoff at 40 500 cm^{-1}. Where there is no subscript. the difference is relative to the lower convergence wavefunction. S is the spatial symmetry of the state. The results are presented in cm^{-1}. Powers of 10 are given in parentheses.

	Resonances					CAP matrix convergence				Basis convergence		
	E	$\Gamma/2$	ΔE	$\Delta\Gamma/2$	%	δE_a	δE_b	$\delta\Gamma_a/2$	$\delta\Gamma_b/2$	δE	$\delta\Gamma/2$	S
1	38 661.82	2.40(−2)	0.14	8.77(−3)	60	0.00	0.01	−1.30(−3)	−2.10(−3)			A_1
2	38 669.66	1.69(−2)	0.10	4.37(−3)	80	0.00	0.01	0.00(0)	−9.00(−4)	−0.12	−2.78(−2)	A_1
3	**38 685.19**	**5.24(−6)**	**0.00**	**1.43(−6)**	**60**	0.00	0.00	0.00(0)	−1.00(−8)	−0.01	−2.39(−6)	A_1
4	38 691.04	6.85(−2)	0.31	1.66(−2)	60	−0.20	−0.02	9.90(−3)	9.00(−3)	−0.18	−1.36(−1)	A_1
5	**38 706.55**	**9.71(−4)**	**0.00**	**8.49(−4)**	**60**	0.00	0.00	−5.90(−5)	−2.90(−5)	−0.01	−1.09(−4)	B_1
6	**38 712.97**	**7.02(−3)**	**0.00**	**0.00(0)**	**20**	−0.07	−0.06	−6.18(−3)	−7.18(−3)	−0.06	−4.68(−3)	B_1
7	38 722.37	9.95(−2)	0.32	1.59(−2)	40	0.28	−0.03	2.17(−2)	−2.50(−3)	0.37	−3.20(−1)	B_1
8	38 730.15	1.92(−2)	0.11	4.38(−3)	60	0.00	−0.01	−1.00(−4)	−7.00(−4)	−0.12	−5.60(−3)	B_1
9	38 738.25	4.38(−2)	0.00	0.00(0)	20	0.23	−0.32	−4.10(−2)	−8.80(−3)	0.04	−9.00(−4)	B_1
10	38 738.56	5.18(−2)	0.11	4.92(−3)	40	−0.03		−1.00(−3)		−0.14	−1.23(−2)	B_1
11	**38 753.24**	**8.13(−6)**	**0.00**	**5.55(−7)**	**60**	0.00	0.00	−1.00(−8)	−1.00(−8)	0.00	−9.97(−6)	A_1
12	**38 754.08**	**7.95(−3)**	**0.03**	**3.64(−3)**	**60**	0.00	0.00	1.30(−4)	1.70(−4)	−0.01	8.80(−4)	B_1
13	38 754.50	6.13(−2)	0.50	6.48(−2)	80	0.03	0.04	−5.90(−3)	−4.40(−3)	−0.11	2.39(−2)	B_1
14	**38 767.79**	**2.33(−3)**	**0.00**	**1.60(−3)**	**100**	0.00	0.00	−3.80(−4)	−3.80(−4)	−0.01	−3.20(−4)	B_1
15	38 773.96	2.50(−2)	0.03	1.71(−2)	100	0.00	0.00	−8.00(−4)	−7.00(−4)	0.00	−1.20(−3)	B_1
16	38 778.59	2.65(−2)	0.10	1.56(−2)	80	−0.04	0.01	4.60(−3)	2.50(−3)	−0.04	−3.04(−2)	B_1
17	**38 781.48**	**4.50(−3)**	**0.01**	**2.53(−3)**	**60**	0.01	0.00	−8.40(−3)	−2.30(−4)	−0.02	−4.75(−3)	B_1
18	38 811.89	2.81(−2)	0.00	1.52(−3)	80	0.00	0.00	0.00(0)	0.00(0)	0.01	−8.00(−4)	A_1
19	38 830.02	5.01(−2)	0.00	3.39(−3)	80	0.00	0.00	0.00(0)	0.00(0)	−0.02	−3.00(−4)	A_1
20	38 887.53	5.64(−2)	0.00	1.35(−3)	60	0.00	0.00	1.40(−2)	1.00(−4)	0.01	−1.00(−2)	B_1
21	38 891.23	6.77(−2)	0.02	2.77(−2)	60	0.01	0.00	−1.38(−2)	−2.00(−4)	0.02	−1.42(−2)	A_1
22	38 918.44	8.61(−2)	0.04	4.00(−2)	40	−0.01	0.01	1.40(−3)	−2.00(−3)	0.13	−4.19(−2)	A_1
23	38 952.73	3.63(−2)	0.03	1.60(−2)	100	0.01	0.01	4.00(−3)	3.90(−3)	0.00	−1.20(−3)	B_1
24	**38 978.91**	**2.58(−3)**	**0.00**	**1.58(−3)**	**60**	0.00	0.00	−1.00(−5)	−2.00(−5)	−0.02	−1.42(−3)	B_1

leading to wavefunctions that differ very slightly from the starting eigenvector ϕ. This is confirmed by examining the modulus of the coefficients $c_n^i(\lambda)$ in Eq. (3). Table V shows the coefficients associated with resonant states, both labeled by the order of the original basis elements. States labeled 3 and 11 in Table IV are resonant states Ψ_5 and Ψ_{16} in Table V. It shows that the square modulus of the coefficients c_n^5 and c_n^{16}, associated with those particular resonant states, is particularly close to 1, whereas the remaining coefficients are all very small. To help visualize these resonances, Fig. 4 shows plots of the basis elements ϕ_5 and ϕ_{16}, associated with narrow resonances 3 and 11, respectively, along with basis element ϕ_3 which appears to be associated with resonance 2 in Table IV, and basis element ϕ_{14} which has a relatively low association with Ψ_{14}, a broad A_1 resonance at 38 743.7 cm^{-1} with half-with of 0.21 cm^{-1}.

The basis elements ϕ_5 and ϕ_{16}, associated with 3 and 11, have almost no symmetric stretch excitation, a characteristic akin to the so called horseshoe states[10,48] which fundamentally are high asymmetric stretch excitations. State 2 has basis element ϕ_3 associated with it through a coefficient $c_n^3 = 0.945\,41$, which is fairly high. It appears though that due to the presence of a symmetric stretch excitation, the half-width of this resonant state is significantly larger than either 3 or 11. Basis element ϕ_{14} displays what appears to be a high symmetric stretch excitation and simultaneously is associated with a broad resonance with width of 0.21 cm^{-1}. These observations suggest that basis elements with low symmetric stretch excitations may provide an indication for the energy of resonant states and a qualitative notion of their width.

A feature of the narrow resonances 3 and 11 is that they display very good wavefunction convergence and very

TABLE V. Value of the coefficients c_n^i, associated with basis elements ϕ_i of the resonant states $\Psi_n(\lambda=\lambda_{op})$. Four coefficients are chosen to be such that $\Psi_i(\lambda=0)=\phi_i$ for $i=3$, 5, 14, and 16. Resonances Ψ_3, Ψ_5, and Ψ_{16} correspond to resonances 2, 3, and 11 in Table IV, whereas Ψ_{14} is a broad resonance with $E=38\,743.7$ cm^{-1} and $\Gamma/2=0.21$ cm^{-1}. λ is given in cm^{-1}. Powers of 10 are given in parentheses.

	$\Psi_3(\lambda=65)$	$\Psi_5(\lambda=69)$	$\Psi_{14}(\lambda=57)$	$\Psi_{16}(\lambda=67)$
$\lvert c_n^3\rvert^2$	0.945 41(00)	0.859 64(−09)	0.170 66(−05)	0.445 50(−10)
$\lvert c_n^5\rvert^2$	0.814 63(−01)	1.000 00(00)	0.160 52(−09)	0.389 49(−14)
$\lvert c_n^{14}\rvert^2$	0.458 54(−05)	0.214 22(−09)	0.379 14(−00)	0.161 22(−07)
$\lvert c_n^{16}\rvert^2$	0.107 13(−01)	0.457 94(−15)	0.198 94(−08)	1.000 00(00)

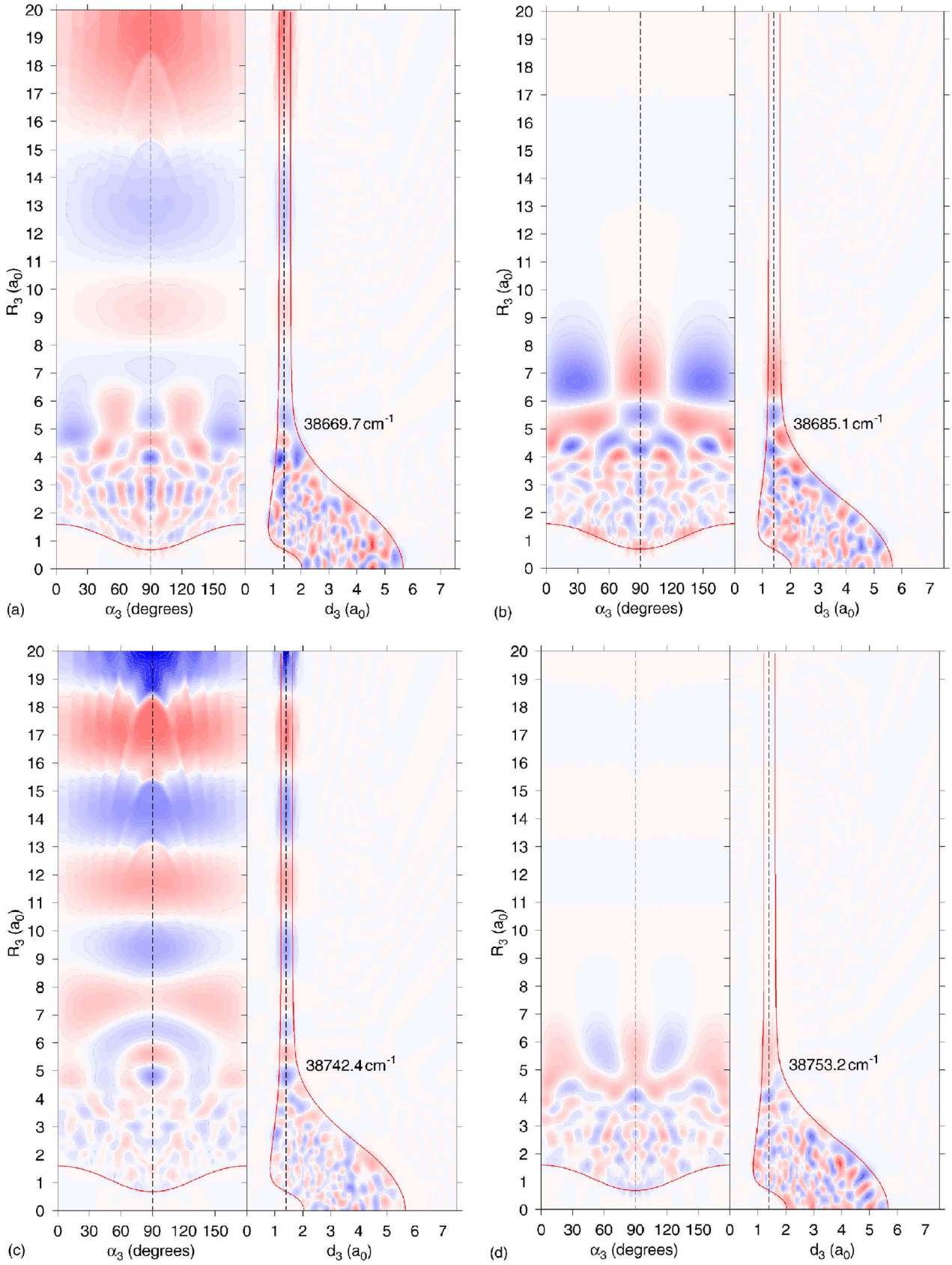

FIG. 4. (Color online) Two-dimensional plots of two sections of the A_1 D_2H^+ basis elements ϕ_i that correspond to (a) broad resonance 2 in Table IV, (b) narrow resonance 3 in Table IV, (c) broad resonance $E=38\,743.7$ cm^{-1} and $\Gamma/2=0.21$ cm^{-1}, and (d) narrow resonance 11 in Table IV. These basis elements are associated with the coefficients c_n^3, c_n^5, c_n^{14}, and c_n^{16} in Table V, respectively. The solid contour shows the classical turning surface. Shades of red show the negative part of the eigenvector, the darker the deeper, whereas shades of blue the positive part. The amplitude of the eigenvector is normalized to 1 in each plot, two panels show two different two-dimensional cuts of the wavefunction, and the dotted line indicates where the two sections intersect. Oscillations in large R_3 regions are fitting artifacts due to the sparsity of the angular grid.

TABLE VI. Results and convergence of H_3^+ vibrational resonant states. States in boldface are within the lifetime range of the observed predissociation spectrum. The columns are position of the resonance E, resonance half-width $\Gamma/2$, uncertainty in the position due to consistency ΔE, uncertainty in half-width due to consistency $\Delta\Gamma/2$, detection percentage %, and the C_{2v} symmetry of the state S. The results are presented in cm^{-1}. Powers of 10 are given in parentheses.

	Resonances					CAP matrix convergence				Basis convergence		
	E	$\Gamma/2$	ΔE	$\Delta\Gamma/2$	%	δE_a	δE_b	$\delta\Gamma_a/2$	$\delta\Gamma_b/2$	δE	$\delta\Gamma/2$	S
1	39 288.16	2.90(−2)	0.09	2.20(−2)	55.6	0.00	0.00	−1.00(−7)	−2.00(−7)	−0.16	−3.16(−5)	B_1
2	39 288.21	3.50(−2)	0.00	7.74(−3)	22.2	0.00	0.00	0.00(0)	0.00(0)	−0.20	−1.30(−3)	A_1
3	39 303.89	7.71(−2)	0.09	1.93(−2)	22.2	0.00	0.00	0.00(0)	0.00(0)			B_1
4	39 342.65	9.77(−2)	0.00	1.75(−2)	22.2	−0.01	0.01	3.00(−4)	2.10(−3)			A_1
5	39 344.07	5.42(−2)	0.02	3.94(−2)	22.2	0.00	0.00	0.00(0)	0.00(0)	−0.11	−1.27(−1)	B_1
6	**39 374.52**	**2.56(−3)**	**0.00**	**2.25(−3)**	**44.4**	0.01	0.01	−1.40(−3)	−3.00(−3)	1.24	−1.13(−2)	A_1
7	39 391.20	5.68(−2)	0.00	0.00(0)	11.1	0.00	0.00	−1.00(−5)	3.90(−4)	−1.23	−9.26(−1)	A_1
8	39 396.39	2.83(−2)	0.00	0.00(0)	11.1	0.00	0.22	0.00(0)	5.07(−2)	−0.63	5.58(−2)	B_1
9	39 397.27	812(−2)	0.01	2.88(−2)	44.4	−0.93	−0.07	−1.02(−1)	−1.36(−2)			B_1
10	39 420.42	8.86(−2)	0.00	0.00(0)	11.1	0.00	0.01	−4.00(−4)	1.07(−2)	−1.62	−7.33(−1)	A_1
11	39 431.44	2.91(−2)	0.01	1.29(−2)	22.2	1.06	0.01	−1.21(−0)	−7.50(−3)			B_1
12	39 435.86	6.77(−2)	0.00	3.12(−3)	22.2	0.00	0.01	0.00(0)	8.20(−3)			B_1
13	39 436.02	6.14(−2)	0.01	4.43(−3)	44.4	−0.14	0.00	6.27(−2)	0.00(0)	−0.14	6.76(−2)	B_1
14	39 469.14	1.02(−2)	0.00	5.66(−3)	33.3	0.00	0.00	0.00(0)	1.30(−3)	−0.19	1.09(−2)	A_1
15	39 478.00	8.19(−2)	0.12	6.67(−2)	55.6	0.00	0.00	−4.00(−4)	−1.10(−3)			A_1
16	39 488.00	9.07(−2)	0.07	6.07(−2)	55.6	0.01	0.01	−3.81(−2)	−2.30(−3)	−0.05	−1.72(−1)	B_1
17	39 503.97	6.65(−2)	0.05	2.65(−2)	33.3	0.02	0.00	−1.53(−2)	−5.00(−4)	−1.46	−5.16(0)	B_1
18	**39 514.85**	**1.16(−3)**	**0.00**	**8.99(−4)**	**44.4**	−0.02	−0.06	2.70(−3)	−1.38(−2)			A_1
19	39 523.38	6.34(−2)	0.02	2.40(−2)	33.3	0.00	0.00	−3.00(−4)	−1.40(−4)	1.89	−1.57(0)	B_1
20	39 552.30	2.01(−2)	0.00	6.78(−4)	22.2	0.00	0.02	−2.00(−4)	−9.80(−3)	−0.28	−7.84(−1)	A_1
21	**39 552.89**	**3.83(−3)**	**0.00**	**5.04(−4)**	**33.3**	0.00	0.00	0.00(0)	5.50(−3)	0.77	−4.67(−1)	B_1
22	39 571.29	2.06(−2)	0.01	1.27(−2)	33.3	0.00	0.00	3.00(−5)	−3.00(−5)	−0.04	−9.62(−2)	A_1
23	**39 604.79**	**1.15(−3)**	**0.00**	**1.52(−4)**	**33.3**	0.00	0.00	−6.30(−3)	−1.33(−2)			B_1
24	39 605.15	8.61(−2)	0.01	2.06(−2)	44.4	−0.80	0.00	−1.58(−1)	1.00(−5)	−0.50	−1.53(−1)	A_1
25	39 667.57	9.75(−2)	0.00	1.28(−3)	33.3	0.00	0.00	0.00(0)	2.00(−4)	−2.76	−1.64(0)	B_1
26	39 720.22	2.10(−2)	0.00	1.43(−2)	77.8	0.00	0.01	0.00(0)	2.29(−2)			B_1
27	39 725.55	4.29(−2)	0.00	3.02(−2)	66.7	0.00	0.00	−2.10(−3)	0.00(0)	−0.20	−3.60(−2)	B_1
28	39 744.32	2.75(−2)	0.00	1.94(−3)	55.6	0.00	0.00	−6.10(−3)	−6.00(−3)	1.19	−2.33(−1)	B_1
29	**39 745.83**	**3.92(−3)**	**0.00**	**2.41(−4)**	**33.3**	0.00	0.00	−2.00(−4)	−7.00(−4)			A_1
30	39 786.87	6.13(−2)	0.01	3.91(−2)	55.6	0.00	0.00	0.00(0)	−1.00(−5)	−1.64	−1.29(−1)	B_1
31	**39 850.87**	**3.09(−3)**	**0.00**	**2.59(−5)**	**22.2**	0.00	0.00	−1.16(−2)	−9.50(−3)	−1.99	−2.66(−1)	B_1
32	39 891.62	6.34(−2)	0.01	1.69(−3)	33.3	0.00	0.00	0.00(0)	−7.00(−5)			B_1
33	39 926.18	7.14(−2)	0.00	1.06(−2)	33.3	0.00	0.01	−8.00(−4)	−1.80(−3)			A_1
34	39 975.55	1.29(−2)	0.02	7.95(−3)	55.6	0.00	0.00	1.00(−4)	−5.00(−4)	0.96	4.51(−2)	B_1
35	40 054.03	4.63(−2)	0.00	1.50(−3)	44.4	0.00	0.00	0.00(0)	−5.00(−4)	1.26	−3.73(−1)	B_1
36	40 184.40	8.22(−2)	0.01	5.38(−3)	44.4	0.00	0.03	1.00(−4)	2.28(−2)	−0.15	−1.47(−2)	A_1
37	**40 325.60**	**3.42(−3)**	**0.00**	**3.29(−4)**	**44.4**	0.00	0.00	4.00(−4)	150(−3)	0.99	−4.98(−1)	B_1

strong consistency in their detection. This can be easily explained by the low coupling that these states have with the remaining basis elements, as indicated by Table V.

We note that there are no resonance widths narrower than 0.01 cm^{-1} above the D^++HD dissociation threshold. This may be due to the fact that both H^++D_2 and D^++HD channels are open, which naturally increases the probability of dissociation, reducing resonant lifetimes. However, the behavior of the resonance widths in this region suggests that the widths may be overestimated and may require larger CAP basis sets to fully converge them.

B. H_3^+ vibrational resonances

The results for the H_3^+ vibrational resonances with half-width narrower than 0.1 cm^{-1} and respective convergence results are presented in Table VI. They were calculated using 592 basis elements for A_1 states and 570 basis elements for B_1 states, from the energy region 39 273–43 300 cm^{-1}. Nine CAPs with Δr ranging from 2 to 10 a_0 in steps of 1 a_0 were calculated, setting r_2 to 21.56 a_0. A total of 252 candidate resonances was identified in the energy range 39 273–40 273 cm^{-1}, of which 48 have consistency in Δr above 60%. The wavefunctions with 120 radial points had the furthermost grid point in the dissociation coordinate R at 19.91 a_0. Therefore, we maintained the same CAP parameters as the largest calculation.

Unlike the resonances calculated for D_2H^+, these resonances show larger widths and less consistency in the narrowest half-widths. The results appear to have worse wavefunction convergence than the ones obtained for D_2H^+. This

TABLE VII. Results for $J=3$ H_3^+ resonant states in cm^{-1}. The columns are position of the resonance E, resonance half-width $\Gamma/2$, uncertainty in the position due to consistency ΔE, uncertainty in half-width due to consistency $\Delta\Gamma/2$, detection percentage %, and S is the C_{2v} symmetry symmetry of the state. Powers of 10 are given in parentheses.

	E	$\Gamma/2$	ΔE	$\Delta\Gamma/2$	%	S		E	$\Gamma/2$	ΔE	$\Delta\Gamma/2$	%	S
1	39 280.05	4.82(−2)	0.12	2.52(−2)	60	A_2	22	39 501.64	1.65(−2)	0.00	2.50(−3)	60	A_2
2	39 288.57	3.48(−2)	0.06	1.52(−2)	100	A_2	23	39 504.24	1.50(−2)	0.00	1.41(−3)	60	A_2
3	39 293.63	1.23(−2)	0.00	0.00(0)	20	B_2	24	39 511.78	1.61(−2)	0.00	1.13(−4)	40	A_2
4	39 299.35	1.08(−2)	0.01	5.36(−3)	80	A_2	25	39 513.03	2.61(−2)	0.00	3.27(−4)	40	A_2
5	39 302.80	7.49(−3)	0.01	1.83(−3)	80	A_2	26	39 534.13	9.38(−3)	0.00	9.49(−5)	40	A_2
6	39 327.05	1.73(−2)	0.01	1.14(−2)	100	A_2	27	39 542.25	4.91(−2)	0.01	1.47(−2)	60	A_1
7	39 335.59	1.21(−2)	0.01	6.55(−3)	100	A_2	28	39 547.30	5.40(−2)	0.08	1.21(−2)	80	B_1
8	39 339.51	3.70(−2)	0.03	1.89(−2)	80	A_2	29	39 549.40	1.17(−2)	0.00	0.00(0)	20	A_1
9	39 346.79	9.03(−3)	0.00	1.35(−2)	100	A_1	30	39 550.06	6.96(−2)	0.02	7.89(−3)	40	B_1
10	39 354.59	4.33(−2)	0.03	2.77(−2)	80	A_2	31	39 553.74	2.91(−2)	0.00	1.69(−3)	60	A_2
11	39 355.57	4.28(−3)	0.00	0.00(0)	20	A_2	32	39 558.37	1.91(−2)	0.00	0.00(0)	20	A_1
12	39 395.19	3.18(−4)	0.00	7.98(−6)	40	A_2	33	39 558.70	8.52(−3)	0.00	1.64(−5)	40	A_2
13	39 399.53	2.63(−2)	0.00	7.63(−4)	40	A_2	34	39 575.62	2.05(−2)	0.00	4.51(−3)	60	A_2
14	39 411.34	9.22(−2)	0.14	4.05(−2)	80	B_1	35	39 576.80	2.65(−2)	0.00	3.64(−3)	60	A_2
15	39 438.28	6.45(−3)	0.00	2.63(−3)	80	A_1	36	39 584.40	1.30(−2)	0.00	4.20(−4)	40	A_2
16	39 447.63	4.98(−2)	0.02	1.53(−2)	80	B_1	37	39 606.89	2.65(−2)	0.00	3.81(−3)	40	A_2
17	39 456.76	4.22(−2)	0.00	7.40(−5)	40	A_2	38	39 615.16	1.83(−2)	0.00	1.73(−3)	60	A_2
18	39 470.23	2.52(−2)	0.00	4.66(−4)	60	A_2	39	39 654.58	7.00(−2)	0.01	1.84(−2)	40	B_1
19	39 475.83	3.39(−3)	0.00	0.00(0)	20	B_1	40	39 795.06	4.80(−2)	0.20	1.22(−1)	100	A_1
20	39 495.56	4.37(−2)	0.01	3.91(−3)	40	A_2	41	40 016.57	6.94(−2)	0.01	1.31(−2)	60	B_1
21	39 500.71	2.78(−2)	0.01	4.10(−3)	80	B_1	42	40 309.21	4.94(−2)	0.01	1.71(−2)	40	A_2

may be due to the large jump in wavefunction parameters between the largest and smallest H_3^+ calculation.

States pairs (1,2), (20,21), and (28,29) in Table VI appear to be degenerate pairs with E symmetry from the D_{3h} group which occur in both A_1 and B_1 symmetries of the C_{2v} group, as discussed in Sec. III A. Because of the finite basis set, their energies are not quite identical. This energy splitting can also be used as a measure of convergence.[49]

C. H_3^+ $J=3$ resonance results

Table VII presents results for $J=3$ H_3^+ calculations including Coriolis coupling effects and using all the basis elements with corresponding eigenvalues between 39 273 and 43 300 cm^{-1}. The calculations were performed over all four C_{2v} group symmetries, resulting in a total of 893 candidate resonances in the energy range 39 273–40 273 cm^{-1}, 571 of which are consistent to more than 60% in Δr, defined by five values ranging from 4 to 8 a_0. The resonance widths obtained in this case are of the same order of magnitude as the $J=0$ H_3^+ results, due to their still being substantially Feshbach nature. For $J=3$, the rotational barrier is not sufficiently high to trap shape resonances.[10] Nevertheless, the fact that some of these Feshbach-type resonances fall within the lifetimes observed in the predissociation spectrum of H_3^+ indicates that states with low angular momentum must be studied to fully characterize this dense spectrum.

V. CONCLUSION

We employ a complex absorbing potential L^2 method with a new automated procedure to find stability points in the complex plane associated with resonant states. This automation enables a consistency and uncertainty analysis of energies and half-widths to be performed for each candidate resonance. We find a number of very well converged, narrow, Feshbach-type resonances for D_2H^+ with $J=0$ and for H_3^+ with both $J=0$ and $J=3$. Thus, in addition to shape resonances, Feshbach-type resonances may also play a role in the Carrington-Kennedy predissociation spectrum of H_3^+ and its isotopologues. The present study suggests that all angular momentum quantum numbers that support bound vibrational states should be investigated to gain a full understanding of this spectrum.

ACKNOWLEDGMENTS

This project was funded by the EPSRC under the ChemReact Computing Consortium. We thank the HPC*x* support team for their help as well as Hemal Varambhia and Igor Kozin for very useful discussions and assistance.

[1] R. Prosmiti, O. L. Polyansky, and J. Tennyson, Chem. Phys. Lett. **273**, 107 (1997).
[2] O. L. Polyansky, R. Prosmiti, W. Klopper, and J. Tennyson, Mol. Phys. **98**, 261 (2000).
[3] J. Tennyson, Rep. Prog. Phys. **57**, 421 (1995).
[4] P. Drossart, J. P. Maillard, J. Caldwell, S. J. Kim, J. K. G. Watson, W. A. Majewski, J. Tennyson, S. Miller, S. Atreya, J. Clarke, J. H. Waite, Jr., and R. Wagener, Nature (London) **340**, 539 (1989).
[5] A. Carrington, J. Buttenshaw, and R. A. Kennedy, Mol. Phys. **45**, 753 (1982).
[6] A. Carrington and R. A. Kennedy, J. Chem. Phys. **81**, 91 (1984).
[7] A. Carrington, I. R. McNab, and Y. D. West, J. Chem. Phys. **98**, 1073 (1993).
[8] M. J. Bramley, J. W. Tromp, T. Carrington, Jr., and G. C. Corey, J. Chem. Phys. **100**, 6175 (1994).
[9] V. A. Mandelshtam and H. S. Taylor, J. Chem. Soc., Faraday Trans. **93**, 847 (1997).
[10] E. Pollak and C. Schlier, Acc. Chem. Res. **22**, 223 (1989).
[11] J. J. Munro, J. Ramanlal, J. Tennyson, and H. Y. Mussa, Mol. Phys. **104**, 115 (2006).

[12] M. Berblinger, J. M. Gomez-Llorente, E. Pollak, and C. Schlier, Chem. Phys. Lett. **146**, 353 (1988).
[13] A. V. Chambers and M. S. Child, Mol. Phys. **65**, 1337 (1988).
[14] M. Berblinger, C. Schlier, and E. Pollak, J. Phys. Chem. **93**, 2319 (1989).
[15] J. M. Gomez-Llorente and E. Pollak, J. Chem. Phys. **90**, 5406 (1989).
[16] J. R. Henderson and J. Tennyson, Mol. Phys. **89**, 953 (1996).
[17] J. J. Munro, J. Ramanlal, and J. Tennyson, New J. Phys. **7**, 196 (2005).
[18] P. Barletta, B. C. Silva, J. J. Munro, and J. Tennyson, Mol. Phys. **104**, 2801 (2006).
[19] H.-D. Meyer, J. Horáek, and L. S. Cederbaum, Phys. Rev. A **43**, 3587 (1991).
[20] Y. Sajeev and P. Sourav, *Current Topics in Atomic, Molecular and Optical Physics* (World Scientific, Singapore, 2006), pp. 187–198.
[21] H. Y. Mussa and J. Tennyson, Chem. Phys. Lett. **366**, 449 (2002).
[22] A. U. Hazi and H. S. Taylor, Phys. Rev. A **1**, 1109 (1970).
[23] J. Aguilar and J. M. Combes, Commun. Math. Phys. **22**, 269 (1971).
[24] E. Balslev and J. M. Combes, Commun. Math. Phys. **22**, 280 (1971).
[25] B. Simon, Ann. Math. **97**, 247 (1973).
[26] R. Kosloff and D. Kosloff, J. Comput. Phys. **63**, 363 (1986).
[27] J. Muga, J. Palao, B. Navarro, and I. Egusquiza, Phys. Rep. **395**, 357 (2004).
[28] W. Meyer, P. Botschwina, and P. G. Burton, J. Chem. Phys. **84**, 891 (1986).
[29] U. V. Riss and H.-D. Meyer, J. Phys. B **26**, 4503 (1993).
[30] N. Moiseyev, S. Friedland, and P. R. Certain, J. Chem. Phys. **74**, 4739 (1981).
[31] S. Skokov, J. M. Bowman, and V. A. Mandelshtam, Phys. Chem. Chem. Phys. **1**, 1279 (1999).
[32] A. Callegari and T. R. Rizzo, Chem. Soc. Rev. **30**, 214 (2001).
[33] B. Poirier and T. Carrington, Jr., J. Chem. Phys. **118**, 17 (2003).
[34] B. Poirier and T. Carrington, Jr., J. Chem. Phys. **119**, 77 (2003).
[35] D. E. Manolopoulos, J. Chem. Phys. **117**, 9552 (2002).
[36] T. Gonzalez-Lezana, E. J. Rackham, and D. E. Manolopoulos, J. Chem. Phys. **120**, 2247 (2004).
[37] O. Shemer, D. Brisker, and N. Moiseyev, Phys. Rev. A **71**, 032716 (2005).
[38] J. Tennyson, M. A. Kostin, P. Barletta, G. J. Harris, J. Ramanlal, O. L. Polyansky, and N. F. Zobov, Comput. Phys. Commun. **163**, 85 (2004).
[39] M. A. Kostin, O. L. Polyansky, and J. Tennyson, J. Chem. Phys. **116**, 7564 (2002).
[40] M. A. Kostin, O. L. Polyansky, J. Tennyson, and H. Y. Mussa, J. Chem. Phys. **118**, 3538 (2003).
[41] J. J. Munro, Ph.D. thesis, University of London, 2006.
[42] M. Ashworth, I. J. Bush, M. F. Guest, A. G. Sunderland, S. Booth, J. Hein, L. Smith, K. Stratford, and A. Curioni, Concurrency Comput.: Pract. Exper. **17**, 1329 (2005).
[43] A. Aguado, O. Roncero, C. Tablero, C. Sanz, and M. Paniagua, J. Chem. Phys. **112**, 1240 (2000).
[44] L. P. Viegas, A. Alijah, and A. J. C. Varandas, J. Chem. Phys. **126**, 074309 (2007).
[45] N. Moiseyev, Phys. Rep. **302**, 212 (1998).
[46] G. Drolshagen, F. A. Gianturco, and J. P. Toennies, Isr. J. Chem. **29**, 417 (1989).
[47] C. Schlier and U. Vix, Chem. Phys. **95**, 401 (1985).
[48] J. Tennyson and J. R. Henderson, J. Chem. Phys. **91**, 3815 (1989).
[49] J. R. Henderson, J. Tennyson, and B. T. Sutcliffe, J. Chem. Phys. **98**, 7191 (1993).
[50] R. J. Le Roy, 2002, University of Waterloo, Chemical Physics Research Report CP-655, http://scienide.uwaterloo.ca/~leroy/level/.